

Article

Effects of Commonly Occurring Metal Ions on Hydroxyapatite Crystallization for Phosphorus Recovery from Wastewater

Hongliang Dai ^{1,2} , Xinwei Tan ¹, Hui Zhu ¹, Tongshuai Sun ¹ and Xingang Wang ^{1,*}

¹ School of Environmental and Chemical Engineering, Jiangsu University of Science and Technology, No. 2 Mengxi Road, Zhenjiang 212018, China; daihongliang103@163.com (H.D.); tc01143@163.com (X.T.); 18252588451@163.com (H.Z.); 18252588460@163.com (T.S.)

² School of Energy and Environment, Southeast University, No. 2 Sipailou Road, Nanjing 210096, China

* Correspondence: hofs@just.edu.cn or hofs@163.com; Tel.: +86-0511-8563-5850

Received: 26 September 2018; Accepted: 7 November 2018; Published: 9 November 2018



Abstract: Hydroxyapatite crystallization for phosphorus recovery and removal from wastewater has attracted considerable attention for its potential economic and environmental benefits because hydroxyapatite can be used as an effective compound fertilizer containing phosphorus (P) for industrial and agricultural applications. As hydroxyapatite is obtained through precipitation and crystallization from wastewater, it is important to evaluate the roles of metal ions commonly found in wastewater during the hydroxyapatite crystallization process. Batch crystallization experiments were conducted to investigate the influence of Mg^{2+} , Fe^{3+} , Cu^{2+} , and Zn^{2+} on P removal efficiency, and crystallized products were characterized using scanning electron microscopy as well as energy dispersive spectroscopy and X-ray diffraction. The presence of Mg^{2+} improved the phosphorus removal rate, but hydroxyapatite crystalline purity was reduced due to the co-precipitation of struvite and hydroxyapatite. Fe^{3+} and Cu^{2+} did not significantly affect the crystalline structure of hydroxyapatite because the two metal ions easily formed hydroxyl metal compounds with low solubility in alkaline solution, which is rarely involved directly in the hydroxyapatite crystallization process. There was strong background interference from Zn^{2+} on the hydroxyapatite X-ray diffraction spectra, indicating that the crystallized products comprised a mixture of several amorphous substances. A comprehensive understanding of the effects of metal ions on hydroxyapatite crystallization will help improve the quality of hydroxyapatite products recovered from wastewater.

Keywords: hydroxyapatite; crystallization; metal ions; phosphorus recovery; wastewater

1. Introduction

Phosphorus (P) is not only a limited and non-renewable mineral resource that makes a major contribution to agricultural and industrial development [1], but also the main element for causing water eutrophication [2,3]. With the decreasing availability of P resources and increasing demand for water environmental quality, the recovery and removal of P from wastewater have drawn great attention [4–6]. Urban domestic sewage contains abundant P; therefore, 15–20% of the world's P demand is theoretically satisfied by recovering and recycling P from wastewater [7]. The recovery of P from sewage can prevent eutrophication in water bodies, and recycling P resources carries economic and environmental benefits [2–10].

Currently, several technologies have been applied to P removal and recovery from wastewater [9,11,12]. One approach is the crystallization of P via the formation of struvite (or magnesium ammonium phosphate (MAP), $MgNH_4PO_4$) and hydroxyapatite (HAP, $Ca_5(PO_4)_3OH$),

which is economical and efficient, providing effective P recovery and high-quality crystallization products [2,10,13,14]. MAP crystallization can remove P and ammonia nitrogen simultaneously and is often used to recover nutrients from anaerobic digestion supernatant, pig wastewater, landfill leachate, and urine because it requires a high ammonia nitrogen concentration and high pH [15–17]. MAP crystallization is unsuitable for P recovery from municipal sewage because the concentration of ammonia nitrogen in municipal sewage is too low. However, HAP crystallization has a wide range of applications for treating P-containing wastewater at different concentrations and is especially suitable for the recovery of P from anaerobic sedimentation tank effluent (~20 mg/L) during the enhanced biological P removal (EBPR) process [2,10].

HAP is a sparingly soluble salt ($K_{sp} = 2.35 \times 10^{-59}$, 25 °C) [18]. Theoretically, the principal chemical reaction for the formation of HAP is based on the following reaction:



As shown in Equation (1), the crystallization process is strongly dependent on pH and the molar ratio of calcium (Ca)/P [19]. Therefore, the pH and Ca/P level of the solution are frequently employed to investigate HAP crystallization behavior [10]. The HAP crystallization process includes nucleation and crystal growth, which are affected by physicochemical factors such as pH, supersaturation, Ca/P, temperature, mixing, and impurity ions. However, few studies have focused on the influences of metal ions on HAP crystallization. Municipal sewage has a wide range of sources and complex components [20]. There are many kinds of metal ions in such sewage, which may affect the process of phosphorus recovery from sewage by HAP crystallization. Therefore, it is important to study the mechanism of P recovery from wastewater by HAP crystallization in the presence of typical metal ions.

The P crystallization process includes nucleation and crystal growth processes affected by various factors such as the pH, supersaturation ratio, temperature, and mixing, and by the existence of foreign ions [21]. Among these factors, few studies have focused on the influences of foreign ions on the P crystallization process [22–26]. Madsen [24] investigated the inhibition behavior of Cu^{2+} and Zn^{2+} on crystal growth and the morphology of brushite ($\text{CaHPO}_4 \cdot 2\text{H}_2\text{O}$), and the results showed that both two metal ions demonstrated strong inhibitory effects on the crystallization of brushite. Muryanto and Bayuseno [25] found that both Zn^{2+} and Cu^{2+} inhibited struvite crystallization, with Zn^{2+} acting as a more effective antiscalant for struvite control. Yan and Shih [21] quantitatively evaluated the effects of Ca^{2+} and Fe^{3+} on struvite crystallization, and the results indicated that both Ca^{2+} and Fe^{3+} significantly inhibited the formation of struvite crystals and modified the needle-like struvite into irregular shapes. In our previous study, Fe^{3+} and Cu^{2+} increased the metastable zone width of HAP crystallization due to the adsorption of these impurity ions on the crystal surface, resulting in an increase in the energy level required for crystal product precipitation, effectively creating an energy barrier for crystallization [26].

Previous studies have focused mainly on identifying the characteristics of struvite and brushite products in the presence of metal ions, with less research on the phase composition and structure of HAP precipitates. In this study, we explored the optimal initial pH and Ca/P ratio for HAP crystallization, and four metal ions (Mg^{2+} , Fe^{3+} , Cu^{2+} , and Zn^{2+}) common in municipal sewage were selected to observe their effects on HAP crystallization at different concentrations. The results of this study will improve the current understanding of the HAP crystallization mechanism and provide a promising approach for the effective recovery of quality HAP products from wastewater as a renewable nutrient resource.

2. Materials and Methods

2.1. Experimental Apparatus and Design

P recovery in the form of HAP crystallization from anaerobic supernatant of the Enhanced Biological Phosphorus Removal (EBPR) process was performed in a batch beaker. The temperature

and stirring rate of the reaction system were controlled using a digital magnetic stirrer (LUXI 85-2W, Shanghai Luxi Industrial Co., Ltd., Shanghai, China) with a heating function. The Oxidation-Reduction Potential (ORP)/pH of the reaction system was measured using a pH meter (YSI Pro Plus, YSI Co. Ltd., Yellow Springs, OH, USA). The stirring rate and temperature were controlled at 200 rpm and 23 °C, respectively. The reaction system was agitated for 20 min, and then the solutions was precipitated for 2 h, after which the precipitates were filtrated through 0.45- μm filters (Millipore HAWP01300, MA, USA). The precipitates were dried in the drying oven with a temperature of 65 °C for 20 h before the subsequent characteristic analysis [3,8]. The liquor samples were also collected for the P removal efficiency in the form of HAP.

The chemical reagents used in the experiment were of analytical grade. Calcium chloride (CaCl_2), and potassium dihydrogen phosphate (KH_2PO_4) were selected to produce HAP precipitation. In the experiment, 100 mL stock solutions of CaCl_2 (200 mg/L) and KH_2PO_4 (100 mg/L) were agitated in a 1000 mL beaker. The chemical reagents were dissolved in distilled water to prepare stock solutions at a concentration of 0.1 M. To determine the influence of pH, the following pH values were evaluated: 7.0, 7.5, 8.0, 8.5, 9.0, 9.5, 10.0, 10.5, and 11.0. 1 M NaOH solution was added to adjust the mixture solution pH to the designated values. Molar Ca/P ratios of 1:2, 1:1, 1.67:1, and 2:1 were assessed, which have been suggested as HAP crystallization conditions based on a variety of wastewater-derived sources. The changes in phosphorus removal efficiency over 90 min with time were investigated under different molar ratios of Ca/P. $\text{MgCl}_2 \cdot 6\text{H}_2\text{O}$, FeCl_3 , $\text{CuCl}_2 \cdot 2\text{H}_2\text{O}$, and ZnCl_2 were used to investigate the influences of typical metal ions on HAP crystallization. For the metal ion influence experiments, the dosages of four metal ions (Mg^{2+} , Fe^{3+} , Cu^{2+} , and Zn^{2+}) were all designated as 0, 5, 10, 15, 20, and 25 mg/L at the optimized pH and Ca/P ratio.

P-containing wastewater was the simulated anaerobic supernatant of the enhanced biological phosphorus removal (EBPR) process (an anaerobic–anoxic/nitrifying two sludge process) previously established by our group [3]. The detailed components of wastewater used in this experiment were as follows: chemical oxygen demand (COD) of 84.2 ± 4.3 mg/L (CH_3COONa), NH_4^+ -N of 36.5 ± 2.2 mg/L (NH_4Cl), PO_4^{3-} -P of 21.2 ± 1.1 mg/L (KH_2PO_4), and alkalinity of 312 ± 25 mg/L (NaHCO_3).

2.2. Analytical Methods

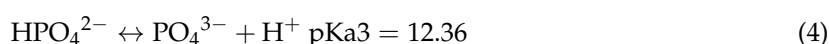
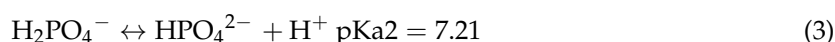
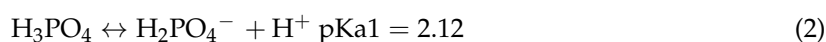
The P concentrations in the sample solution were measured using UV spectrophotometry at 700 nm based on the molybdenum-blue ascorbic acid method [27]. The concentrations of Mg^{2+} , Fe^{3+} , Cu^{2+} , and Zn^{2+} were determined using an atomic absorption spectrometer (PerkinElmer AAS, Waltham Mass, MA, USA) in an air acetylene flame. The crystallized products were ground into powder using an agate mortar before the structure analysis. The morphology and relative content of the components of the crystallized products were determined using scanning electron micrography (SEM) with energy-dispersive spectrometry (EDS) (Hitach S-4800, Ibaraki, Japan). An X-ray diffraction analysis (XRD) for the product structure was carried out utilizing a D8 ADVANCE diffractometer (Bruker AXS, Karlsruhe, Germany) with diffraction patterns in step sizes of 0.02° , ranging from 10° to 65° at a 2θ angle.

3. Results and Discussion

3.1. Effects of Ph on HAP Crystallization

pH is a crucial factor for the HAP crystallization process. HAP crystallization cannot occur spontaneously at low pH due to the low saturation of the reaction system [19]. In contrast, a high-pH solution may be supersaturated, such that homogeneous precipitation can occur easily, which is not conducive to P recovery [26]. The anaerobic supernatant in the EBPR process contains abundant P but is lower in pH than the optimal value for HAP formation [10]. Therefore, it is necessary to optimize the pH of the reaction system for P recovery in the form of HAP. The effects of pH on P removal by HAP crystallization at an initial Ca/P molar ratio of 1.67 are shown in Figure 1. As the pH increased from 7.0 to 11.0, the P removal efficiency exhibited two stages. In the first stage, as the pH increased

from 7.0 to 9.5, the residual P concentration decreased to 0.902 mg/L at a P removal efficiency of 95.15%. The most rapid increase in P crystal products occurred at pH 8–9, at a rate of 15% per 0.5 increase in pH. During the second stage, as the pH increased from 9.5 to 11.0, the P removal efficiency was relatively stable. The residual P concentration decreased by only 0.414 mg/L, and the P removal efficiency increased from 95.15 to 95.66%. The maximum P removal efficiency was 97.73% at pH 10.0, and the residual P content was 0.454 mg/L, which was lower than the first-class A standard (0.5 mg/L) set by the Discharge Standard of Pollutants for Urban Wastewater Treatment Plant (GB 18918-2002). The main reason for the observed pH effects on P removal efficiency was the presence of different forms of dissolved phosphate in the solution, including PO_4^{3-} , HPO_4^{2-} , $\text{H}_2\text{PO}_4^{2-}$, and H_3PO_4 [28]. The equilibrium relationships of these phosphates in water were as follows:



At a low pH, the content of PO_4^{3-} , as a product of the third-order ionization reaction, was lower than that of H_2PO_4^- , the first-order ionization product. As the pH increased, the proportion of PO_4^{3-} increased rapidly, and HAP formation was promoted, leading to an increase in P-removal efficiency. However, Ca^{2+} in solution readily forms $\text{Ca}(\text{OH})_2$ and CaCO_3 precipitate at a high pH; this process directly reduced the concentration of Ca^{2+} in solution and indirectly affected the crystallization reaction. Considering the P removal rate and recovery performance of the crystallized products, pH 9 was selected as the best condition for the reaction system in subsequent experiments.

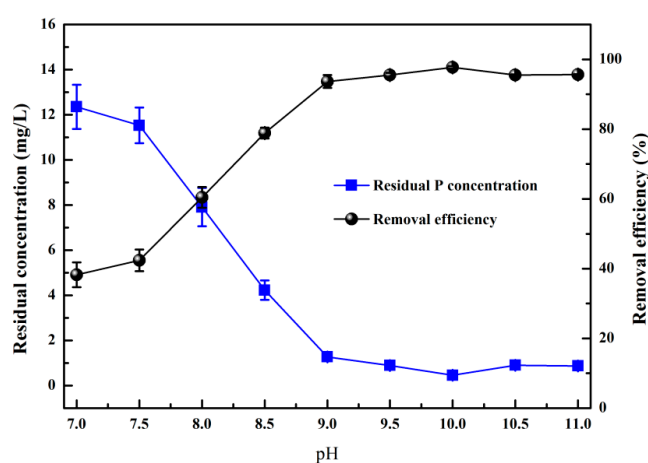


Figure 1. Effect of pH on phosphorus removal by HAP (Hydroxyapatite) crystallization.

3.2. Effects of Ca/P on HAP Crystallization

In the solution of different Ca/P for HAP crystallization, the precursors DCPD (dicalcium phosphate dihydrate, $\text{CaHPO}_4 \cdot 2\text{H}_2\text{O}$), OCP (octacalcium phosphate, $\text{Ca}_8\text{H}(\text{PO}_4)_6 \cdot 5\text{H}_2\text{O}$), and ACP (amorphous calcium phosphate, $\text{Ca}_3(\text{PO}_4)_2 \cdot x\text{H}_2\text{O}$) formed first, and thermodynamically stable HAP was then formed through a series of material structure transformations [10,19]. To investigate the effects of Ca^{2+} concentration on the P removal efficiency, different concentrations of CaCl_2 solution were added simultaneously to alter the Ca/P ratio at pH 9. As shown in Figure 2a, as the Ca/P ratio increased, the P concentration decreased rapidly in the reaction system. When the reaction time was 90 min, the concentration of phosphorus decreased from 20.3 mg/L to 8.32, 4.56, 1.32, and 1.09 mg/L at Ca/P ratios of 1:2, 1:1, 1.67:1, and 2:1, respectively, with P removal efficiency of 58.97%, 77.63%, 93.25%, and 95.59%, respectively (Figure 2b). When the Ca/P molar ratio was greater than 1.67, the excessive Ca concentration in the solution (Ca/P ratio = 2.0) did not significantly increase the P removal efficiency.

CaCO_3 precipitation can occur via the addition of high concentrations of Ca^{2+} in an alkaline environment, permitting easy Ca^{2+} loss and a waste of chemicals [3]. P removal occurred mainly during the first 35 min of the reaction, and the P removal efficiency did not increase significantly after 35 min (Figure 2a). Therefore, the Ca/P ratio was set to 2 and the reaction time to 35 min for subsequent experiments.

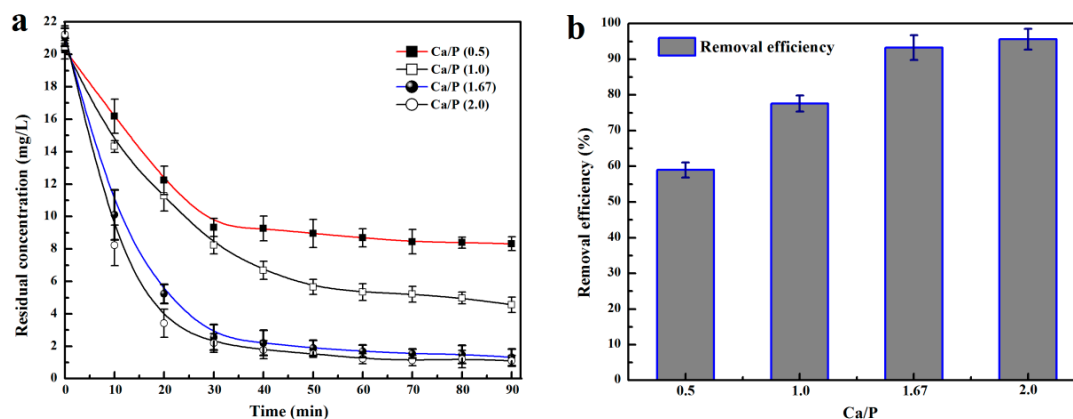


Figure 2. The effects of Ca/P molar ratios on phosphorus removal by HAP crystallization.

3.3. Effects of Metal Ions on the HAP Crystallization

Metal ions in wastewater can have important effects on the physicochemical characteristics of HAP crystallization for P recovery. Several recent studies have investigated the properties of struvite crystallization in the presence of cationic and anionic impurities and found that these impurities can change the morphology and composition of crystallized products [21,25,29,30]. However, the effects of metal ions on HAP crystallization for P recovery have only been reported rarely. The effects of different concentrations of four metal ions (Mg^{2+} , Fe^{3+} , Cu^{2+} , and Zn^{2+}) on the efficiency of P removal by HAP at pH 9.0 and a Ca/P ratio of 2.0 are shown in Figure 3.

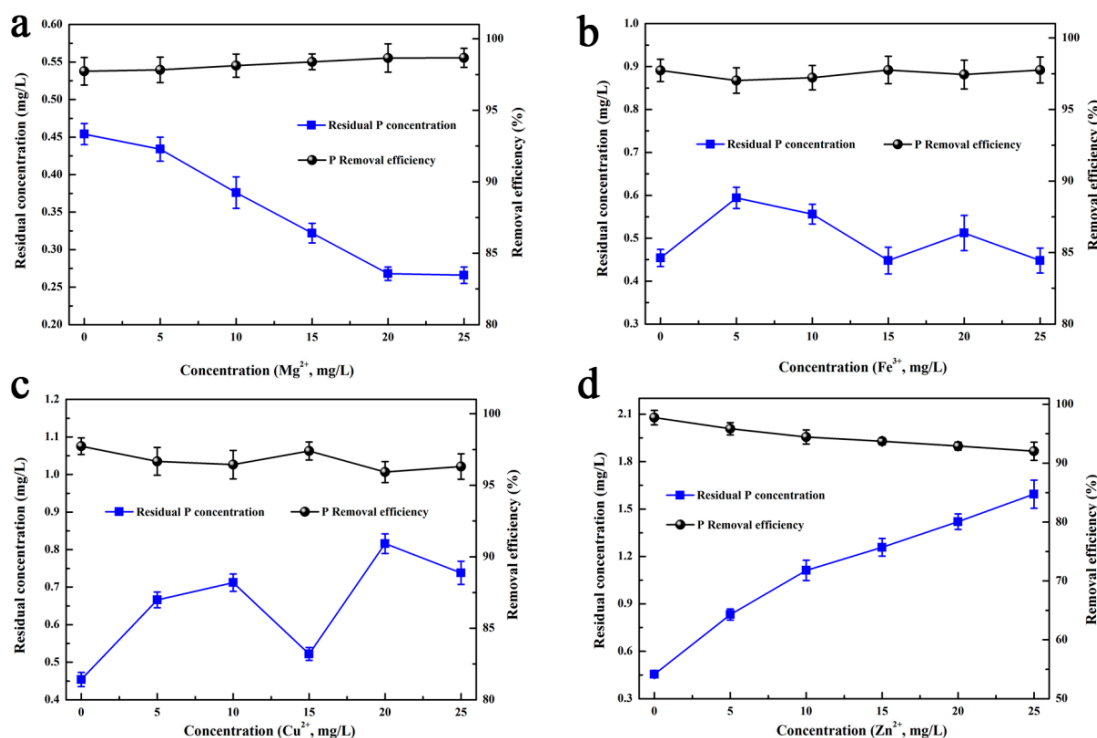
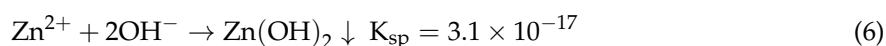
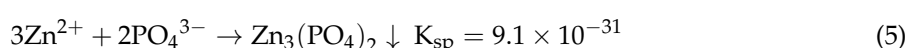


Figure 3. Effects of metal ions on the efficiency of phosphorus removal by HAP crystallization, (a) Mg^{2+} ; (b) Fe^{3+} ; (c) Cu^{2+} ; (d) Zn^{2+} .

As shown in Figure 3a, the residual P concentration decreased from 0.45 to 0.27 as the Mg^{2+} concentration increased from 0 to 25 mg/L. Thus, the addition of Mg^{2+} contributed to the P removal rate (by ~1%), because the presence of PO_4^{3-} , NH_4^+ , and Mg^{2+} in the reaction system made it possible to form MAP, in turn favoring P removal. In contrast, the precipitation of Mg^{2+} in the form of $Mg(OH)_2$ consumed the alkalinity of the solution, making it unsuitable for HAP crystallization under the theoretical optimum pH condition; this phenomenon led to a decrease in the P removal efficiency. These conditions altered the residual P concentration and P crystallization rate in the reaction system.

The solubility of Fe^{3+} in water is limited, and its concentration less than 10 mg/L does not interfere with the chemical properties and functions of the solution [21]. Therefore, a wide range of Fe^{3+} concentration (0–25 mg/L) was chosen to study the role of Fe^{3+} in the crystallization of HAP. As shown in Figure 3b, the addition of Fe^{3+} did not significantly affect P removal from the solution, and the residual P concentration decreased only slightly as the Fe^{3+} concentration increased from 5 to 25 mg/L. Previous studies have shown that Fe^{3+} exists mainly in the form of polyhydroxyl complexes in alkaline solution environments, where it co-precipitates with phosphate, mainly as ferric phosphate and ferric hydroxide. These complexes adsorb phosphate from wastewater to some extent, resulting in a reduction in the P concentration in the solution [21].

Cu^{2+} and Zn^{2+} were selected because the two metal ions are usually present in municipal sewage and piggery wastewater, and previous found that both Cu^{2+} and Zn^{2+} demonstrated strong inhibitory effects on the crystallization of phosphate minerals such as brushite ($CaHPO_4 \cdot 2H_2O$) [24]. Muryanto and Bayuseno [25] investigated struvite crystallization with interference from Cu^{2+} and Zn^{2+} and found that both ions can inhibit struvite crystallization and that Zn^{2+} was a more effective antiscalant for struvite crystallization than Cu^{2+} . As shown in Figure 3c,d, the P removal efficiency could be inhibited by the presence of Cu^{2+} and Zn^{2+} , which was similar to the results presented in Muryanto and Bayuseno's study [25] for MAP crystallization. The P removal efficiency decreased from 97.85 to 95.35% and from 97.73 to 92.03% as the Cu^{2+} and Zn^{2+} concentrations increased from 0 to 25 mg/L, respectively, presumably due to the additive adsorption of molecules or ions onto the crystal surfaces [25]. In contrast, Cu^{2+} and Zn^{2+} can form metal hydroxides in alkaline solution, buffering the alkalinity of the reaction system and leading to a decrease in the P removal efficiency. Zn^{2+} inhibited the P removal efficiency more strongly than Cu^{2+} did because Zn^{2+} is an amphoteric metal, whose form in solution is greatly influenced by pH. In an alkaline solution containing phosphate, Zn^{2+} produces the following chemical reactions:



$Zn(OH)_2$ is an amphoteric hydroxide, and its solubility is related to pH value (Figure 4). When the pH is lower than 8, Zn^{2+} exists mainly in the form of $Zn_3(PO_4)_2$. However, the experiment was conducted at pH 9; thus, large amounts of $Zn_3(PO_4)_2$ began to dissolve and precipitate in the form of $Zn(OH)_2$. These chemical reactions both increased the phosphate content and consumed OH^- in the solution, thus inhibiting HAP crystallization for P removal.

3.4. Effects of Metal Ions on the Characteristics of Crystallized Products

The inhibitory effects of metal ions on the crystallization processes are commonly accompanied by irregular crystal growth, because the adsorption of such ions onto crystal surfaces is not uniform [25]. The XRD patterns of the HAP crystals obtained in the presence of metal ions at different concentrations are shown in Figure 5. All the patterns matched well with the data from the HAP standard powder diffraction database at the International Centre for Diffraction Data (PDF#73-0293). XRD showed that HAP formation was poorly crystalline, mainly due to its small crystallite size and the generation of amorphous Ca phosphate (ACP, OCP, and DCPD) [10,31,32]. It can be inferred that the foreign metal

ions were adsorbed onto the surface of the developing crystals and were thus incorporated into the crystal structure, leading to a poor XRD pattern.

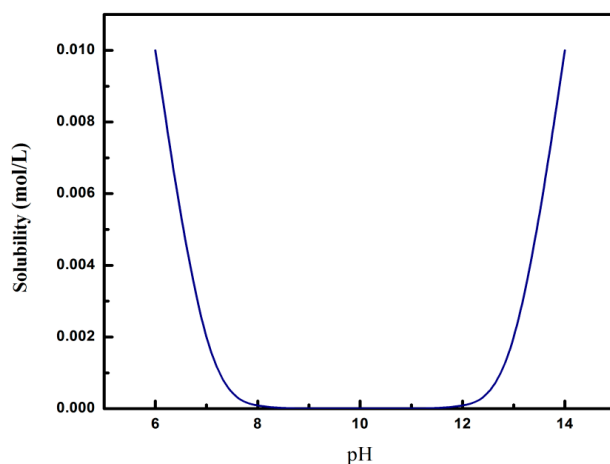


Figure 4. The relation between the solubility of Zn(OH)_2 and pH.

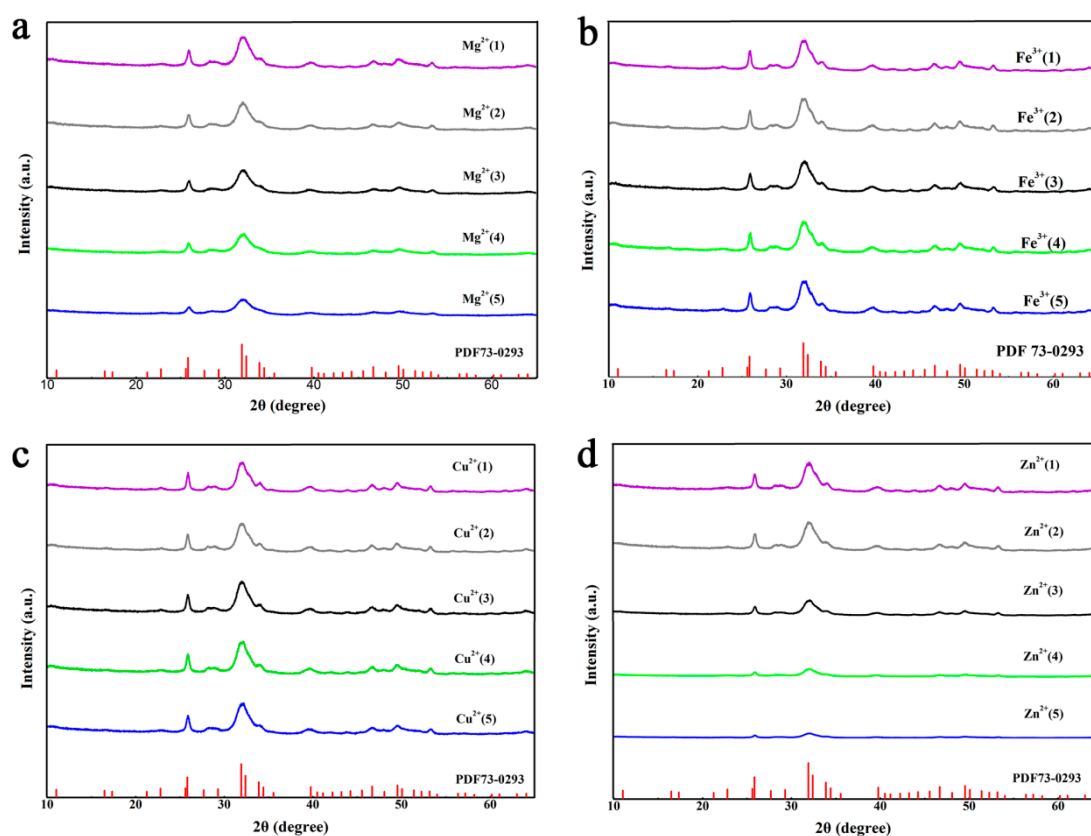


Figure 5. The effects of different concentrations of metal ions on the X-ray diffraction diagrams of HAP crystallized products. (a) Mg^{2+} ; (b) Fe^{3+} ; (c) Cu^{2+} ; (d) Zn^{2+} . The dosages of the metal ions were 5, 10, 15, 20, and 25 mg/L, which correspond to serial numbers 1,2,3,4, and 5, respectively.

The SEM and their associated EDS patterns of the HAP crystals obtained in the presence of several metal ions are shown in Figure 6. The SEM images of the HAP standard shows the typical HAP crystal shape, which is a finely distributed crystalline substance (Figure 6a), which were closely matched with those reported by earlier researchers [3,10,33,34]. To comprehensively evaluate the effects of metal ions on the characteristics of HAP crystallized products, the SEM–EDS images shown in Figure 6c–j in the

presence of metal ions at a concentration of 25 mg/L were selected to represent the variations in HAP morphology and composition.

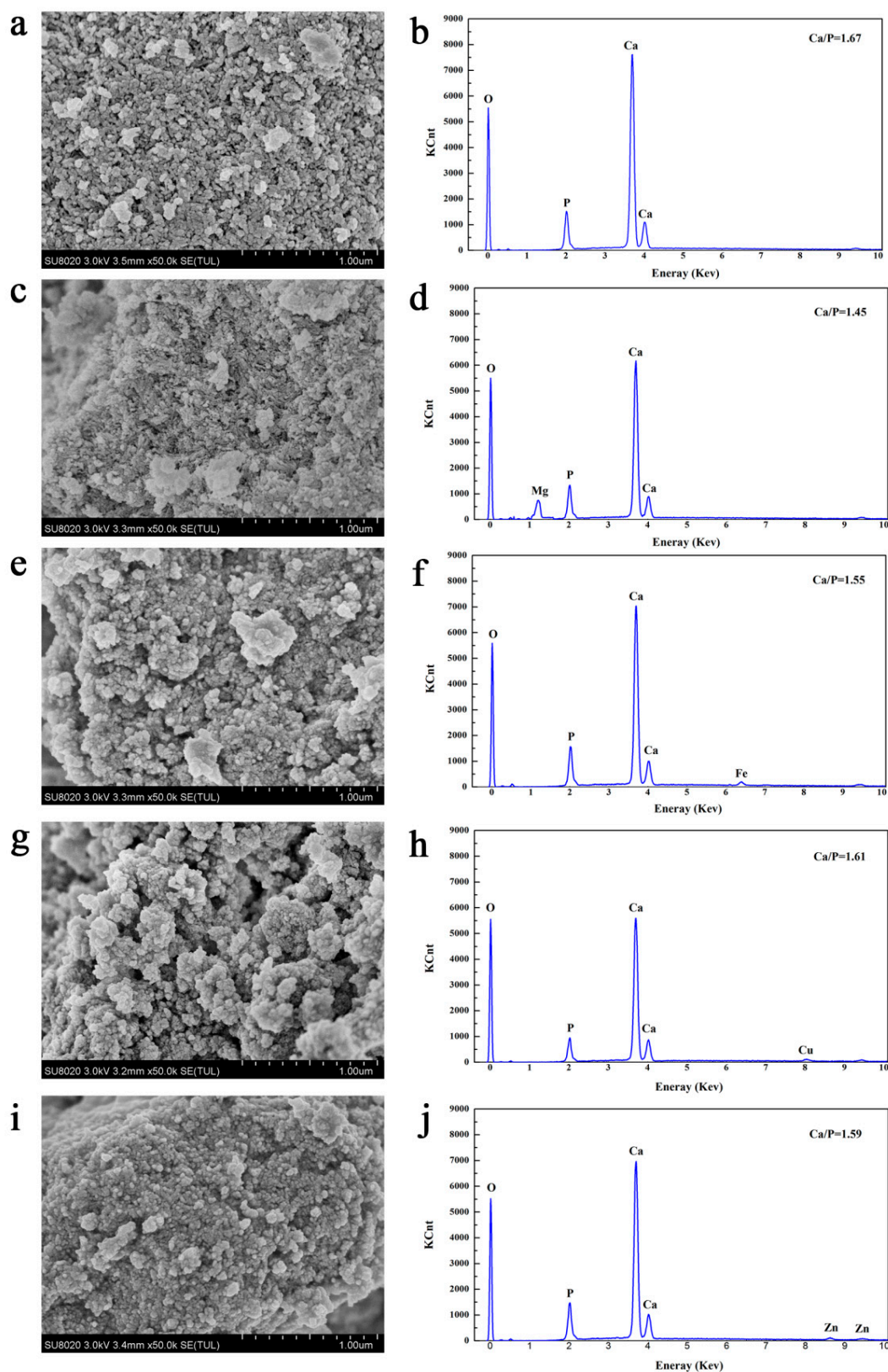


Figure 6. The effects of metal ions on the SEM-EDS of HAP crystallized products (the dosages of the metal ions were 25 mg/L). (a,b) blank sample; (c,d) Mg²⁺; (e,f) Fe³⁺; (g,h) Cu²⁺; (i,j) Zn²⁺.

XRD patterns in Figure 5a showed that HAP was the most clearly detectable phase for precipitates in the presence of Mg^{2+} . The typical intensity of the HAP peak decreased as the Mg^{2+} concentration increased. The SEM diagram in Figure 6c shows that the particle size of HAP crystals decreased, and a small number of needle-like crystals appeared, at an Mg^{2+} concentration of 25 mg/L, indicating that a small amount of struvite crystals formed in the reaction system due to the presence of Mg^{2+} . The elemental composition of the crystal products was quantitatively analyzed using EDS (Figure 6d) and showed that oxygen (O), Ca, and P were the main elements in the samples, and that the Ca/P ratio was lower than the theoretical value for HAP (1.67), indicating that the crystalline products contained amorphous Ca phosphate. The low level of Mg in the EDS spectrum suggested MAP co-precipitation with amorphous Ca phosphate. Although the existence of Mg^{2+} reduced the purity of HAP crystals, it increased the P removal rate in the system.

The presence of Fe^{3+} and Cu^{2+} did not significantly affect the crystal structure of HAP (Figure 5b,c), because Fe^{3+} and Cu^{2+} readily formed low-solubility hydroxyl metal compounds in the alkaline solution. However, Fe^{3+} greatly reduced the concentration of phosphate in the solution, mainly due to precipitation of Fe phosphate, resulting in a decrease in HAP production. This result indicates that Fe^{3+} is an effective inhibitor of HAP crystallization because of its stronger ability to bind to phosphate than that of Ca^{2+} [21]. Luedecke et al. [35] proposed a chemical model to describe the precipitation of ferric hydroxyphosphate by combining phosphate with ferric hydroxide in activated sludge, and found that ferric hydroxyphosphate deposits can be represented by the empirical formula $Fe_{2.5}PO_4(OH)_{4.5}$ with a solubility product constant of 96.7; the corresponding solubility constant for HAP was 58.69. The addition of a small amount of Fe^{3+} had a slight effect on the amount of HAP produced, resulting in an increase in the size of the amorphous crystalline products and a roughening of the structure; this result agreed with those shown in Figure 6e. Compared with Fe^{3+} , Cu^{2+} had a similar effect on HAP crystal morphology. The quantitative analysis of EDS elements showed that in the presence of Fe^{3+} and Cu^{2+} , low levels of Fe and Cu, respectively, were found in the crystalline products, confirming the presence of Fe and Cu salts in addition to Ca phosphate. However, the low level of metal salt ions had no significant effect on the HAP crystal structure.

As shown in Figure 5d, there was strong background interference from Zn^{2+} on the XRD spectrum of HAP, suggesting that the crystallized products contained a mixture of several amorphous substances. When the Zn^{2+} concentration exceeded 20 mg/L, there was almost no obvious HAP crystalline peak. Milky white flocculent precipitates observed during the reaction process suggested that $Zn(OH)_2$ and $Ca(OH)_2$ precipitates had formed in the solution and flocculated with other precipitates, resulting in a mixture of HAP and a variety of amorphous Ca and Zn salts, preventing clear characteristic peaks on XRD. SEM images of HAP under the influence of Zn^{2+} are shown in Figure 6i. The crystalline products exhibited smooth surfaces and dense bulk structures at high Zn^{2+} concentrations, possibly due to a cover of amorphous precursors. As discussed previously, ion impurities are adsorbed onto crystal surfaces, resulting in an energy barrier to crystallization [36]. Compared with the presence of no ion impurities, nucleation requires a greater impetus for crystallization, since a higher energy barrier must be overcome for crystal growth at high concentrations of ion impurities [10].

4. Conclusions

(1) The Ca/P ratio and pH were found to be key factors affecting the P removal rate by HAP crystallization. A rapid increase in the P removal efficiency occurred at pH 8–10, with significant increases in crystallinity and P removal. Higher pH values reversed the reduction in P removal due to the enhanced precipitation effect of $CaCO_3$ and $Ca(OH)_2$. In contrast, the theoretical Ca/P ratio for HAP is 1.67, and the excessive Ca concentration in the solution did not significantly increase the P removal efficiency. $CaCO_3$ precipitation occurred after adding high concentrations of Ca^{2+} to the alkaline environment, which can easily cause Ca^{2+} loss and a waste of chemicals.

(2) The addition of Mg^{2+} and Fe^{3+} reduced the crystalline purity of HAP to some extent but also improved the phosphate removal rate due to the co-precipitation of metal phosphate and HAP. In the

presence of Mg^{2+} , a small amount of needle-like crystals appeared on the surface of the crystalline products due to the formation of small amounts of MAP crystallization products. The addition of Fe^{3+} and Cu^{2+} had no significant effect on the HAP structure because Fe^{3+} and Cu^{2+} readily formed low-solubility hydroxyl metal compounds in the alkaline solution; these are rarely involved in HAP crystallization. There was strong background interference of Zn^{2+} on the XRD spectra of HAP, indicating that the crystallized products may contain a mixture of several amorphous substances. The crystalline products captured on the SEM images at high Zn^{2+} concentrations had smooth surfaces and dense bulk structures, perhaps due to a cover of amorphous precursors.

Author Contributions: The research presented here was carried out as a collaboration between all the authors. H.D. conceived and designed the experiments; X.T. processed the data and carried out the statistical analysis of the results; T.S., H.Z., and X.W. provided suggestions on the methodology and structure of the manuscript.

Funding: This research was funded by the Social Development Project of Zhenjiang [Grant No. 2016014], the Qing Lan Project for Young Core Teachers in University of Jiangsu Province, China, the Natural Science Foundation of Jiangsu Province of China [Grant No. BK2012272], and the Natural Science Foundation of China [Grant No. 31400448].

Acknowledgments: We are very grateful to the editor and three anonymous reviewers for their valuable comments and constructive suggestions that helped us to greatly improve the manuscript.

Conflicts of Interest: The authors declare no conflict of interest.

References

1. Shepherd, J.G.; Sohi, S.P.; Heal, K.V. Optimizing the recovery and reuse of phosphorus from wastewater effluent for sustainable fertilizer development. *Water Res.* **2016**, *94*, 155–165. [[CrossRef](#)] [[PubMed](#)]
2. Conley, D.J.; Paerl, H.W.; Howarth, R.W.; Boesch, D.F.; Seitzinger, S.P.; Havens, K.E.; Lancelot, C.; Likens, G.E. Controlling eutrophication: Nitrogen and phosphorus. *Science* **2009**, *323*, 1014–1015. [[CrossRef](#)] [[PubMed](#)]
3. Dai, H.; Lu, X.; Peng, Y.; Yang, Z.; Zhu, H. Effects of supersaturation control strategies on hydroxyapatite (HAP) crystallization for phosphorus recovery from wastewater. *Environ. Sci. Pollut. Res.* **2017**, *24*, 1–9. [[CrossRef](#)] [[PubMed](#)]
4. Mayer, B.K.; Baker, L.A.; Boyer, T.H.; Drechsel, P.; Gifford, M.; Hanjra, M.A.; Parameswaran, P.; Stoltzfus, J.; Westerhoff, P.; Rittmann, B.E. Total value of phosphorus recovery. *Environ. Sci. Technol.* **2016**, *50*, 6606–6620. [[CrossRef](#)] [[PubMed](#)]
5. Fang, L.; Li, J.S.; Guo, M.Z.; Cheeseman, C.R.; Tsang, D.C.; Donatello, S.; Poon, C.S. Phosphorus recovery and leaching of trace elements from incinerated sewage sludge ash (ISSA). *Chemosphere* **2018**, *193*, 278–287. [[CrossRef](#)] [[PubMed](#)]
6. Cieřlik, B.; Konieczka, P. A review of phosphorus recovery methods at various steps of wastewater treatment and sewage sludge management. The concept of “no solid waste generation” and analytical methods. *J. Clean. Prod.* **2017**, *142*, 1728–1740. [[CrossRef](#)]
7. Yuan, Z.; Pratt, S.; Batstone, D.J. Phosphorus recovery from wastewater through microbial processes. *Curr. Opin. Biotechnol.* **2012**, *23*, 878–883. [[CrossRef](#)] [[PubMed](#)]
8. De-Bashan, L.E.; Bashan, Y. Recent advances in removing phosphorus from wastewater and its future use as fertilizer (1997–2003). *Water Res.* **2004**, *38*, 4222–4246. [[CrossRef](#)] [[PubMed](#)]
9. Qiu, G.; Law, Y.M.; Das, S.; Ting, Y.P. Direct and complete phosphorus recovery from municipal wastewater using a hybrid microfiltration-forward osmosis membrane bioreactor process with seawater brine as draw solution. *Environ. Sci. Technol.* **2015**, *49*, 6156–6163. [[CrossRef](#)] [[PubMed](#)]
10. Dai, H.; Lu, X.; Peng, Y.; Zou, H.; Jing, S. An efficient approach for phosphorus recovery from wastewater using series-coupled air-agitated crystallization reactors. *Chemosphere* **2016**, *165*, 211–220. [[CrossRef](#)] [[PubMed](#)]
11. Okano, K.; Uemoto, M.; Kagami, J.; Miura, K.; Aketo, T.; Toda, M.; Honda, K.; Ohtake, H. Novel technique for phosphorus recovery from aqueous solutions using amorphous calcium silicate hydrates (A-CSHs). *Water Res.* **2013**, *47*, 2251–2259. [[CrossRef](#)] [[PubMed](#)]
12. Egle, L.; Rechberger, H.; Krampe, J.; Zessner, M. Phosphorus recovery from municipal wastewater: An integrated comparative technological, environmental and economic assessment of p recovery technologies. *Sci. Total Environ.* **2016**, *571*, 522–542. [[CrossRef](#)] [[PubMed](#)]

13. Güney, K.; Weideler, A.; Krampe, J. Phosphorus recovery from digested sewage sludge as MAP by the help of metal ion separation. *Water Res.* **2008**, *42*, 4692–4698. [[CrossRef](#)] [[PubMed](#)]
14. Song, Y.; Dai, Y.; Hu, Q.; Yu, X.; Qian, F. Effects of three kinds of organic acids on phosphorus recovery by magnesium ammonium phosphate (MAP) crystallization from synthetic swine wastewater. *Chemosphere* **2014**, *101*, 41–48. [[CrossRef](#)] [[PubMed](#)]
15. Corre, K.S.L.; Valsamijones, E.; Hobbs, P.; Parsons, S.A. Phosphorus recovery from wastewater by struvite crystallization: A review. *Crit. Rev. Environ. Sci. Technol.* **2009**, *39*, 433–477. [[CrossRef](#)]
16. Pastor, L.; Marti, N.; Bouzas, A.; Seco, A. Sewage sludge management for phosphorus recovery as struvite in EBPR wastewater treatment plants. *Bioresour. Technol.* **2008**, *99*, 4817–4824. [[CrossRef](#)] [[PubMed](#)]
17. Kataki, S.; West, H.; Clarke, M.; Baruah, D.C. Phosphorus recovery as struvite: Recent concerns for use of seed, alternative Mg source, nitrogen conservation and fertilizer potential. *Resour. Conserv. Recycl.* **2016**, *107*, 142–156. [[CrossRef](#)]
18. Kumar, R.; Prakash, K.H.; Cheang, P.; Khor, K.A. Temperature driven morphological changes of chemically precipitated hydroxyapatite nanoparticles. *Langmuir* **2004**, *20*, 5196–5200. [[CrossRef](#)] [[PubMed](#)]
19. Song, Y.H.; Weidler, P.G.; Berg, U.; Nüesch, R.; Donnert, D. Calcite-seeded crystallization of calcium phosphate for phosphorus recovery. *Chemosphere* **2006**, *63*, 236–243. [[CrossRef](#)] [[PubMed](#)]
20. Gong, J.; Liu, Y.; Sun, X. O₃ and UV/O₃ oxidation of organic constituents of biotreated municipal wastewater. *Water Res.* **2008**, *42*, 1238–1244. [[CrossRef](#)] [[PubMed](#)]
21. Yan, H.; Shih, K. Effects of calcium and ferric ions on struvite precipitation: A new assessment based on quantitative X-ray diffraction analysis. *Water Res.* **2016**, *95*, 310–318. [[CrossRef](#)] [[PubMed](#)]
22. Ottosen, L.M.; Kirkelund, G.M.; Jensen, P.E. Extracting phosphorus from incinerated sewage sludge ash rich in iron or aluminum. *Chemosphere* **2013**, *91*, 963–969. [[CrossRef](#)] [[PubMed](#)]
23. Li, R.; Zhao, W.; Li, Y.; Wang, W.; Zhu, X. Heavy metal removal and speciation transformation through the calcination treatment of phosphorus-enriched sewage sludge ash. *J. Hazard. Mater.* **2015**, *283*, 423–431. [[CrossRef](#)] [[PubMed](#)]
24. Madsen, H.E.L. Influence of foreign metal ions on crystal growth and morphology of brushite (CaHPO₄·2H₂O) and its transformation to octacalcium phosphate and apatite. *J. Cryst. Growth* **2008**, *310*, 2602–2612. [[CrossRef](#)]
25. Muryanto, S.; Bayuseno, A. Influence of Cu²⁺ and Zn²⁺ as additives on crystallization kinetics and morphology of struvite. *Powder Technol.* **2014**, *253*, 602–607. [[CrossRef](#)]
26. Dai, H.; Lu, X.; Peng, Y.; Yang, Z.; Zhu, H. Characteristics of metastable zone in the crystallization process: A case study of sparingly soluble hydroxyapatite. *Desalin. Water Treat.* **2017**, *62*, 192–199. [[CrossRef](#)]
27. APHA. *Standard Methods for the Examination of Water & Wastewater*, 21st ed.; American Public Health Association, American Water Works Association and Water Environment Federation: Washington, DC, USA, 2005.
28. Monballiu, A.; Desmidt, E.; Ghyselbrecht, K.; Meesschaert, B. Phosphate recovery as hydroxyapatite from nitrified UASB effluent at neutral pH in a CSTR. *J. Environ. Chem. Eng.* **2018**, *6*, 4413–4422. [[CrossRef](#)]
29. Kabdaszli, I.; Parsons, S.A.; Tünaya, O. Effect of major ions on induction time of struvite precipitation. *Croat. Chem. Acta* **2006**, *9*, 243–251.
30. Zheng, X.; Sun, P.; Lou, J.; Fang, Z.; Guo, M.; Song, Y.; Tang, X.; Jiang, T. The long-term effect of nitrite on the granule-based enhanced biological phosphorus removal system and the reversibility. *Bioresour. Technol.* **2013**, *132*, 333–341. [[CrossRef](#)] [[PubMed](#)]
31. Harris, W.G.; Wilkie, A.C.; Cao, X.; Sirengo, R. Bench-scale recovery of phosphorus from flushed dairy manure wastewater. *Bioresour. Technol.* **2008**, *99*, 3036–3043. [[CrossRef](#)] [[PubMed](#)]
32. Combes, C.; Rey, C. Amorphous calcium phosphates: Synthesis, properties and uses in biomaterials. *Acta Biomater.* **2010**, *6*, 3362–3378. [[CrossRef](#)] [[PubMed](#)]
33. Karapinar, N.; Hoffmann, E.; Hahn, H.H. P-recovery by secondary nucleation and growth of calcium phosphates on magnetite mineral. *Water Res.* **2006**, *40*, 1210–1216. [[CrossRef](#)] [[PubMed](#)]
34. Hosni, K.; Moussa, S.B.; Chachi, A.; Amor, M.B. The removal of PO₄³⁻, by calcium hydroxide from synthetic wastewater: Optimisation of the operating conditions. *Desalination* **2008**, *223*, 337–343. [[CrossRef](#)]
35. Luedecke, C.; Hermanowicz, S.W.; Jenkins, D. Precipitation of ferric phosphate in activated sludge: A chemical model and its verification. *Water Sci. Technol.* **1989**, *21*, 325–337. [[CrossRef](#)]

36. Sangwal, K.; Mielniczek-Brzóska, E. Effect of impurities on metastable zone width for the growth of ammonium oxalate monohydrate crystals from aqueous solutions. *J. Cryst. Growth* **2004**, *267*, 662–675. [[CrossRef](#)]



© 2018 by the authors. Licensee MDPI, Basel, Switzerland. This article is an open access article distributed under the terms and conditions of the Creative Commons Attribution (CC BY) license (<http://creativecommons.org/licenses/by/4.0/>).